Applied Physics Letters

Wide range tunable bandgap and composition β-phase $(AlGa)_2O_3$ thin film by thermal annealing

Cite as: Appl. Phys. Lett. **118**, 032103 (2021); https://doi.org/10.1063/5.0027067
Submitted: 27 August 2020 . Accepted: 18 December 2020 . Published Online: 19 January 2021

Che-Hao Liao, Kuang-Hui Li, Carlos G. Torres-Castanedo, Guozheng Zhang, and Xiaohang Li

Applied Physics Letters ARTICLE scitation.org/journal/apl

Wide range tunable bandgap and composition β-phase $(AlGa)_2O_3$ thin film by thermal annealing

Cite as: Appl. Phys. Lett. **118**, 032103 (2021); doi: 10.1063/5.0027067
Submitted: 27 August 2020 · Accepted: 18 December 2020 ·
Published Online: 19 January 2021

Che-Hao Liao,[a] Kuang-Hui Li, Carlos G. Torres-Castanedo, Guozheng Zhang, and Xiaohang Li[a]

AFFILIATIONS

King Abdullah University of Science and Technology (KAUST), Advanced Semiconductor Laboratory, Thuwal 23955, Saudi Arabia

Note: This paper is part of the Special Topic on Ultrawide Bandgap Semiconductors.
[a]**Authors to whom correspondence should be addressed:** chehao.liao@kaust.edu.sa and xiaohang.li@kaust.edu.sa

ABSTRACT

We have demonstrated wide bandgap and composition range β-$(Al_xGa_{1-x})_2O_3$ thin films by employing thermal annealing of β-Ga_2O_3/sapphire templates. With proper annealing conditions at 1000–1500 °C, the β-Ga_2O_3 thin films transformed to the β-$(Al_xGa_{1-x})_2O_3$ thin films with different bandgaps and compositions due to the Al diffusion from sapphire. Meanwhile, the Ga atoms diffused into sapphire. The interdiffusion process caused an increased film thickness, which was enhanced in proportion to the annealing temperature. It was confirmed by secondary ion mass spectrometry (SIMS) and transmission electron microscopy. Thus, higher temperatures resulted in high Al contents in the β-$(Al_xGa_{1-x})_2O_3$ films. Also, the SIMS measurements show highly homogeneous Al contents throughout the β-$(Al_xGa_{1-x})_2O_3$ films annealed at 1200 °C and above. Evaluated by x-ray diffraction (XRD), the Al content range of the samples is 0–0.81 for the β-Ga_2O_3 templates without annealing and with annealing up to 1500 °C. Evaluated by UV-Vis spectroscopy, the optical bandgap range of the samples is 4.88–6.38 eV for the β-Ga_2O_3 templates without annealing and with annealing up to 1400 °C, translating to the Al content range of 0–0.72. Moreover, the crystal quality of β-$(Al_xGa_{1-x})_2O_3$ improved as the Al composition became larger due to higher annealing temperatures. The proposed technique is promising for the preparation of β-$(Al_xGa_{1-x})_2O_3$ thin films without employing "direct-growth" techniques.

III-oxide semiconductors such as Ga_2O_3 have attracted increasing attention recently because of the wide bandgap, excellent stability, and availability of bulk substrates for high-performance deep-ultraviolet (DUV) solar-blind photodetectors (PDs), transparent electronics, and power electronics.[1–15] The monoclinic β-phase is widely recognized as the most stable Ga_2O_3 crystalline structure,[16] amid bulk β-Ga_2O_3 crystal growth[17–19] and thin film deposition.[20–26] For further development of III-oxide optical and power devices, the progress would benefit greatly from the alloy formation, tunability of the alloy composition, and, thereby, the associated properties such as bandgap, absorption spectrum, and breakdown field.[27] In particular, $(Al_xGa_{1-x})_2O_3$ alloys are promising candidates for shorter-wavelength and higher-power devices due to large tunable bandgaps from about 4.9 (β-Ga_2O_3) to above 8.8 eV (α-Al_2O_3).

To form the $(Al_xGa_{1-x})_2O_3$ alloys, researchers have employed RF sputtering,[28] PLD,[29,30] LPCVD,[31] mist-CVD,[32,33] laser MBE,[34,35] MOCVD,[36–39] and MBE.[40] These "direct-growth" techniques offer the tunability of material composition and, thus, bandgap. Since most of those studies concern the β phase, the bandgap and composition ranges of the β-$(Al_xGa_{1-x})_2O_3$ alloys are summarized in Table I. For instance, the bandgap range reported by Shi *et al.* for the β-$(AlGa)_2O_3$ alloys is 6.10 − 6.22 eV by LPCVD.[31] Zhang *et al.* have demonstrated β-$(AlGa)_2O_3$ films deposited by PLD with the wide-range bandgap tunability up to 6.1 eV, above which the X-ray diffraction (XRD) 2θ (−201) and higher-order peaks were almost invisible.[30] Overall, the associated costs of the direct-growth techniques are not trivial because of various requirements: targets with different compositions, high-purity precursors/sources, and demanding environments such as an ultrahigh vacuum.

In the 1990s, Fleischer and Battiston *et al.* discovered that the thermal annealing of Ga_2O_3 films on sapphire could lead to Al diffusion into the films.[41,42] Later, Kokubun *et al.* found that increased temperatures from 600 to 1200 °C during thermal treatment of Ga_2O_3 sol–gel can boost the polycrystalline Ga_2O_3 bandgap from 4.95 to 5.53 eV which the authors attributed to the Al diffusion.[20] Recently, Goyal *et al.* varied annealing temperatures of polycrystalline Ga_2O_3 films on sapphire from 600 to 1000 °C to obtain a changing bandgap from 4.63 to 5.15 eV with an annealing time of 36 h.[43] They performed

TABLE I. Summary of the bandgap and Al content ranges of the β-$(Al_xGa_{1-x})_2O_3$ thin films by various direct-growth techniques and the thermal annealing technique in this work. In the parentheses of the last two columns are the characterization techniques including UV-Vis spectroscopy (UV-Vis), energy-dispersive x-ray spectroscopy (EDS), x-ray photoelectron spectroscopy (XPS), Rutherford backscattering spectrometry (RBS), and XRD.

Technique	Substrate	Bandgap range	Al content range
RF sputtering[28]	*c*-sapphire	5.0–5.4 eV (UV-Vis)	0–0.059 (EDS)
PLD[30]	*c*-sapphire	5.2–6.1 eV (XPS)	0.24–0.76 (XPS)
LPCVD[31]	*c*-sapphire	6.10–6.22 eV (UV-Vis)	0.49–0.52 (XPS)
Laser MBE[34]	*c*-sapphire	4.5–5.5 eV (UV-Vis)	0–0.46 (XRD) 0–0.54 (XPS)
Laser MBE[35]	*c*-sapphire	4.89–5.29 eV (UV-Vis)	0–0.35 (XPS)
MOCVD[36]	*c*-sapphire	4.9–5.52 eV (UV-Vis)	0–0.43 (RBS)
MOCVD[37]	(010) β-Ga_2O_3	NA	0.1–0.20 (XRD, APT)
MOCVD[38]	(100) β-Ga_2O_3	5.1–5.7 eV (XPS) for x = 0.17–0.47 (XRD)	0.1–0.52 (XRD) 0.15–0.48 (EDS)
MOCVD[39]	(−201) β-Ga_2O_3	5.20–5.72 eV (XPS)	0.21–0.48 (XRD, XPS)
MBE[40]	(100) β-Ga_2O_3	NA	0.33–0.61 (XPS)
Annealing (this work)	*c*-sapphire	4.88–6.38 eV for ≤1400 °C (UV-Vis)	0–0.72 for ≤1400 °C (UV-Vis) 0-0.81 for ≤1500 °C (XRD)

secondary ion mass spectrometry (SIMS) analysis, which shows Al diffusion into the films, though being largely inhomogeneous. Those studies hint at a viable pathway of forming $(AlGa)_2O_3$ ternary alloys based on Ga_2O_3/sapphire templates by thermal diffusion, which is low cost and straightforward as opposed to the direct-growth techniques. However, the Al compositions were still low and inhomogeneous in those studies, which greatly hindered the application prospects. Besides, the III-oxide/sapphire interface has not been systematically examined, preventing a good understanding of the diffusion process amid the thermal annealing.

In this work, we report on a wide range bandgap and composition tuning technique of using common β-Ga_2O_3/sapphire templates to obtain ternary β-$(AlGa)_2O_3$ alloys by thermal annealing at various elevated temperatures. We found that controlling annealing temperature from 1000 to 1500 °C can tune the diffusion rate, leading to a large optical bandgap change from 4.88 to 6.38 eV for β-$(Al_xGa_{1-x})_2O_3$. The corresponding material bandgap and film thickness were characterized systematically by multiple techniques. Besides, the thin-film/sapphire interface was investigated by high-resolution transmission electron microscopy (HR-TEM) to understand the interdiffusion process.

The 50-nm thick β-Ga_2O_3 thin-films were deposited on *c*-plane sapphire substrates by the PLD. Although the PLD was utilized, it is important to note that the same studies can be performed for the binary β-Ga_2O_3 films on sapphire grown by other techniques such as CVD, MBE, and MOCVD because we expect that the thermal diffusion could occur regardless of how the β-Ga_2O_3/sapphire templates are prepared. The PLD conditions include a heater temperature of 800 °C, a chamber pressure of 4.5 mTorr, and a KrF (248 nm) excimer laser power of 400 mJ with a repetition rate of 5 Hz. An undoped Ga_2O_3 target of 99.99% purity provided by Sigma-Aldrich was employed. Thermal annealing was conducted in an MTI KSL-1700X-A4-DC furnace at different temperatures of 1000 − 1500 °C with the step of 100 °C in air at atmospheric pressure for three hours. The ramp rate for the annealing process is +4 °C/min below 800 °C and increased to +5 °C/min (above 800 °C); the cooling rate is −5 °C/min down to 200 °C. The crystal structures, material quality, material composition, optical properties, thin film thickness, and interface were characterized by using XRD, SIMS, optical UV-Vis transmission, and TEM. The XRD 2θ-ω scans were carried out using a Bruker D2 PHASER system with a wavelength of $\lambda = 1.5406$ Å. The SIMS experiments for elemental depth profiling were performed using a Dynamic SIMS system from Hiden Analytical. The optical transmission was measured using a Shimadzu UV-3600 spectrophotometer. The TEM specimens were obtained using a Helios focused ion beam (FIB) system. The cross-sectional TEM images and EDX mapping were acquired using an FEI Titan ST system with a Gatan EDX module.

Figure 1 shows the XRD 2θ-ω scan spectra of the as-deposited and annealed Ga_2O_3 thin films on sapphire with different annealing temperatures. For the as-deposited Ga_2O_3 sample, there are three dominating peaks from (−201) and higher-order diffraction planes of β-Ga_2O_3 film. The samples annealed at 1000 and 1100 °C manifest only the main (−201) and higher order (−402) and (−603) peaks for

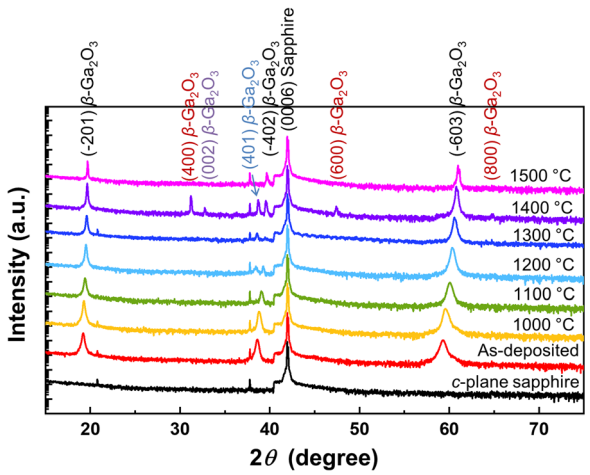

FIG. 1. XRD 2θ-ω scan spectra of the as-deposited and annealed Ga_2O_3 thin films on sapphire with different annealing temperatures of 1000–1500 °C and a bare sapphire substrate as the reference.

TABLE II. XRD 2θ-ω scan peak positions of different diffraction planes extracted from Fig. 1 and the calculated lattice parameters and Al contents of the β-$(Al_xGa_{1-x})_2O_3$ samples annealed at various temperatures. The contents estimated from the UV-Vis measurement from Fig. 3 are shown in the last column for comparison.

Sample	−201 (°)	−402 (°)	−603 (°)	*a* (Å)	*b* (Å)	*c* (Å)	*β* (°)	x XRD	x UV-Vis
As deposited	18.92	38.36	59.02	12.21	3.04	5.81	103.87	0.00	0.00
1000 °C	19.00	38.54	59.29	12.17	3.03	5.79	103.90	0.10	0.26
1100 °C	19.12	38.83	59.79	12.06	2.99	5.75	103.98	0.35	0.50
1200 °C	19.23	39.01	60.04	12.01	2.98	5.73	104.02	0.48	0.60
1300 °C	19.33	39.19	60.28	11.96	2.96	5.71	104.06	0.60	0.65
1400 °C	19.37	39.28	60.51	11.91	2.95	5.69	104.09	0.71	0.72
1500 °C	19.43	39.40	60.71	11.87	2.93	5.67	104.12	0.81	NA

the β phase. When the temperature increases to 1200–1400 °C, the (−402) peak splits into two peaks: one remains the (−402) peak and the other might be the (401) peak. For the 1400 °C annealed sample, several extra peaks such as (002) and (400) and the higher order peaks were observed, which could be attributed to the lattice rotation or tilting due to thermal strain induced by high temperature annealing.[44] However, for the 1500 °C sample, those peaks disappeared, indicating good crystallinity. Figure S1 in the supplementary material shows XRD phi-scan of the (−401) plane of the as-deposited β-Ga_2O_3 sample and three β-$(AlGa)_2O_3$ samples annealed at 1000, 1200, and 1400 °C. All exhibit sixfold symmetry diffraction peaks, which demonstrate the single β phase.

Table II summarizes the positions of the (−201) and higher-order (−402) and (−603) peaks in Fig. 1. They shift toward higher angles as the annealing temperature increases from 1000 to 1500 °C, suggesting reduced lattice constants and, thus, increased Al contents. Based on Bragg's law and the positions of the (−603) peaks, the *d* spacings were calculated for the samples. Then, using the lattice parameter formulas of β-$(Al_xGa_{1-x})_2O_3$ from the study by Kranert *et al.*,[45] $a = (12.21 - 0.42x)$ Å, $b = (3.04 - 0.13x)$ Å, $c = (5.81 - 0.17x)$ Å, $\beta = (103.87 + 0.31x)^o$, and Eq. (1),[34] the Al content x values were calculated, as shown in Table II. They manifest a wide range from 0 to 0.81 for the β-$(Al_xGa_{1-x})_2O_3$ samples thanks to the thermal annealing,

$$\frac{1}{d^2} = \frac{h^2}{a^2\sin^2\beta} + \frac{k^2}{b^2} + \frac{l^2}{c^2\sin^2\beta} - \frac{2hl\cos\beta}{ac\sin^2\beta}. \quad (1)$$

Table S1 shows the crystal quality and the surface roughness of the samples. The crystal quality of β-$(AlGa)_2O_3$ improves proportional to the annealing temperature and, thus, the Al content. The XRD (−201) rocking curve (RC) FWHM drops from 2.51° for as-deposited Ga_2O_3 to 0.15° for the β-$(AlGa)_2O_3$ sample annealed at 1500 °C. This is in marked contrast to the previous works by direct-growth techniques where the crystallinity and crystal quality generally deteriorated when the Al content in the β-$(AlGa)_2O_3$ alloys increased.[30,31,38] The surface roughness probed by 5×5 μm^2 atomic force microscopy (AFM) scan remains less than 2 nm for the annealing temperatures from 1000 to 1400 °C. But for the 1500 °C annealed sample, the surface starts to decompose due to high temperature, making the surface roughness non-uniform across the sample surface.

The SIMS measurements were carried out by depth profiling of Al, Ga, and O elements for the as-deposited and annealed samples at 1000, 1200, and 1400 °C shown in Fig. 2. Figure 2(a) shows that the Al concentration of as-deposited Ga_2O_3 is at or below the detection limit level, indicating minimal Al diffusion at the PLD temperature of 800 °C. Also, the figure shows that the Ga_2O_3 film thickness is 50 nm. With the annealing at 1000 °C, significant Al diffusion occurred unambiguously, as shown in Fig. 2(b). The annealing also increased the film thickness to 110 nm, indicating that the interdiffusion process of Ga and Al atoms occurred at the III-oxide/sapphire interface. However, there is a small gradient of Ga and Al concentrations throughout the film. Thus, the alloy material composition is not strictly homogeneous for this sample. With higher temperatures of 1200 and 1400 °C, the film thickness increased further to 190 and 250 nm, respectively, suggesting stronger interdiffusion shown in Figs. 2(c) and 2(d). More importantly, the Al concentrations are highly homogeneous throughout the films for both samples, indicating that the samples with annealing temperatures of 1200 °C or higher would possess a homogeneous

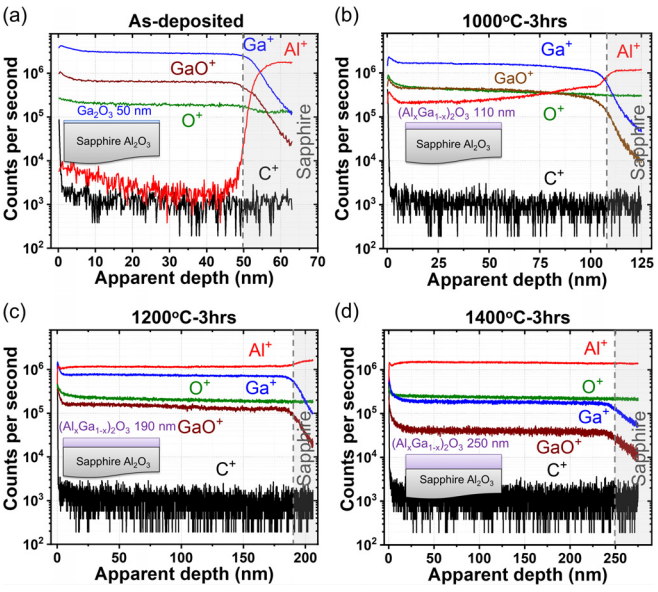

FIG. 2. The SIMS profiles of (a) as-deposited β-Ga_2O_3 and the samples annealed at (b) 1000 °C, (c) 1200 °C, and (d) 1400 °C. The inset shows the sample structures with the estimated film thickness of each sample. The gray dashed lines represent the III-oxide/sapphire interface.

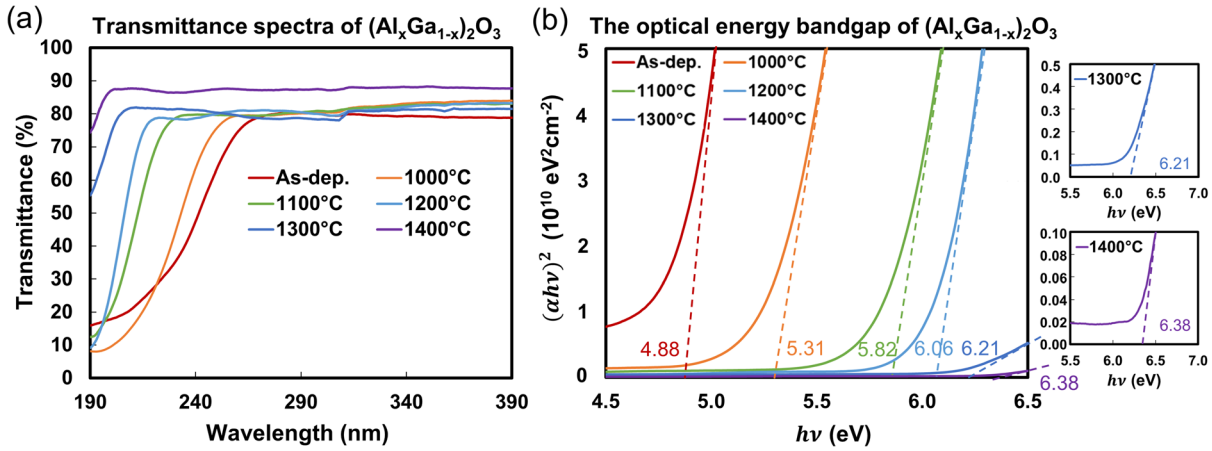

FIG. 3. (a) Transmission spectra and (b) The $(\alpha h\nu)^2$ vs $h\nu$ Tauc plots and the optical energy bandgap extrapolations of the as-deposited β-Ga_2O_3 and the samples annealed at temperatures of 1000–1400 °C. The insets are enlarged for the 1300 and 1400 °C annealed samples. The sample annealed at 1500 °C could not be measured due to the larger optical bandgap.

composition. The carbon signals in Figs. 2(a)–2(d) appear to be below the detection limit, indicating the low impurity level and, thus, low contamination amid the processes.

To measure the optical bandgap and, thus, the composition of the samples, the UV-Vis transmission measurement was conducted, as shown in Fig. 3(a). The blueshift in the absorption edge with higher annealing temperature can be observed, which suggests the increased Al composition in good agreement with the XRD experiments. Because the minimum detection wavelength is 190 nm, the transmission curves of the samples annealed at 1300 and 1400 °C are less complete. Also, it was not possible to obtain the absorption edge of the sample annealed at 1500 °C due to an even larger bandgap, which is, thus, not included in Fig. 3. Nevertheless, the bandgaps of the annealed samples at 1400 °C and below were first deduced from the Tauc plot shown in Fig. 3(b) calculated from the transmission spectra. Then, the bandgaps were determined by extrapolating linear regions of these curves to the horizontal axis. An increase in the bandgap with annealing temperature was observed. The optical bandgaps for as-deposited β-Ga_2O_3 and annealed β-$(Al_xGa_{1-x})_2O_3$ at 1000, 1100, 1200, 1300, and 1400 °C are 4.88, 5.31, 5.82, 6.06, 6.21, and 6.38 eV, respectively.

Based on Figs. 2 and 3, the relationships of the film thickness vs temperature and the optical bandgap vs temperature show the quasi-linear behavior in Fig. 4(a). This suggests that the annealing temperature is an excellent knob to control the two important thin film quantities. Another potential knob is the annealing time, which is worth further investigation. Subsequently, the Al contents of β-$(Al_xGa_{1-x})_2O_3$ were estimated by the equation $E_g(x) = (1-x)\,E_g(\beta\text{-}Ga_2O_3) + x\,E_g(\theta\text{-}Al_2O_3) - bx(1-x)$ eV. The bandgap E_g values of monoclinic β-Ga_2O_3 and θ-Al_2O_3 are 4.88 and 7.24 eV, and the bowing parameter b is 0.93 eV.[46,47] The Al contents of the annealed β-$(AlGa)_2O_3$ films at 1000,

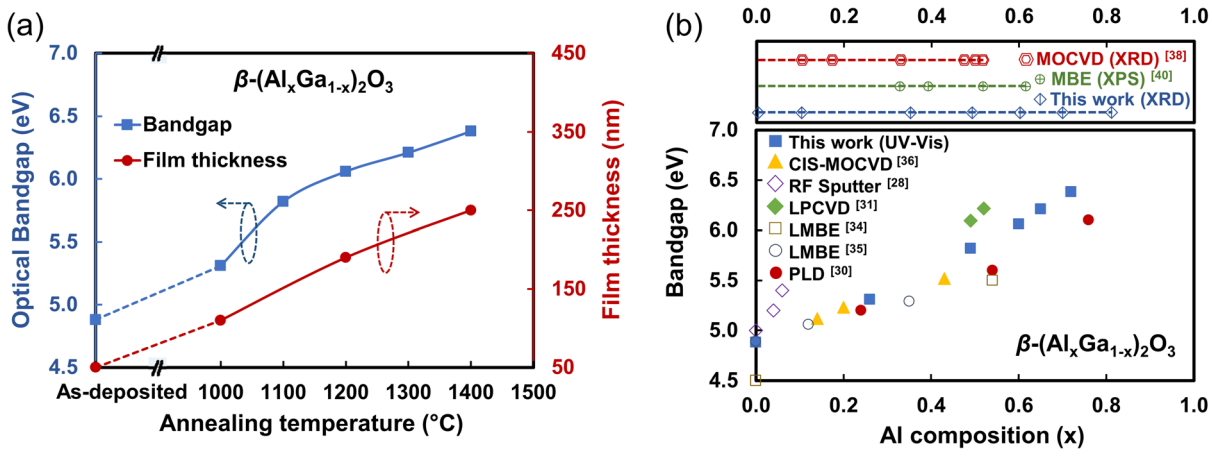

FIG. 4. (a) Optical bandgap and film thickness of the β-$(Al_xGa_{1-x})_2O_3$ films as a function of the annealing temperature. (b) The optical bandgap of the β-$(Al_xGa_{1-x})_2O_3$ film as a function of the Al content estimated by the optical bandgap of this work and the bandgap as a function of the Al content reported by others, where the bandgaps are all optical measured by UV-Vis except that the bandgap in Ref. 30 was measured by XPS. The three horizontal dashed lines above show the Al contents determined by XRD and XPS in Refs. 38 and 40 and the Al contents determined by XRD in this study as references of some of the largest Al contents reported for β-$(Al_xGa_{1-x})_2O_3$ to date.

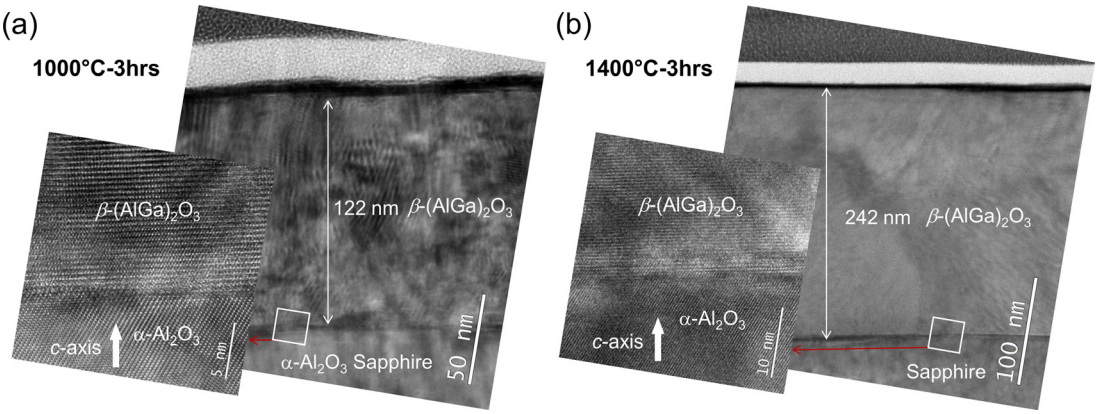

FIG. 5. Cross-sectional TEM images of the samples annealed at (a) 1000 °C and (b) 1400 °C with the insets showing the III-oxide/sapphire interface.

1100, 1200, 1300, and 1400 °C are 0.26, 0.50, 0.60, 0.65, and 0.72, respectively. These Al contents estimated from the UV-Vis measurements are included in Table II for comparison with the ones estimated from the XRD experiments. It appears that the two sets have considerable discrepancy at lower annealing temperatures of 1000–1200 °C but show good agreement at higher annealing temperatures of 1300 and 1400 °C. Figure 4(b) compares the optical bandgap vs the Al content estimated from the optical bandgap of this work with those reported by others using various direct-growth techniques.[28,31,34–36] The result shows that the proposed method possesses the largest optical bandgap tuning ranging from 4.88 to 6.38 eV for the β-$(AlGa)_2O_3$ alloys.

To investigate the III-oxide/sapphire interface, we performed cross-sectional TEM experiments of the samples annealed at 1000 and 1400 °C shown in Fig. 5. Figures 5(a) and 5(b) show the thicknesses of the samples annealed at 1000 and 1400 °C, which are 122 and 242 nm, consistent with the SIMS experiments in Figs. 2(b) and 2(d), respectively. According to the insets of Figs. 5(a) and 5(b), there is a thin transition layer between β-$(AlGa)_2O_3$ and sapphire.

To further study the interface of the two samples in Fig. 5, the cross-sectional HR-TEM images were obtained in the vicinity of the interface shown in Figs. 6(a) and 6(c). The transition layers around 3.6 nm and 4.5 nm thick at the β-$AlGa_2O_3$/sapphire interface can be identified for the 1000 and 1400 °C annealed samples, respectively. The fast Fourier transform (FFT) diffraction patterns below and above the transition layers of both samples confirm the α-phase corundum crystal structure for the sapphire substrate and the monoclinic β-phase crystal structure for the β-$(AlGa)_2O_3$ films. The FFT diffraction patterns of the transition layers of both samples, however, show the mixed α-phase and β-phase.

The STEM HAADF images and EDX maps of the two samples in the vicinity of the interface are shown in Figs. 6(b) and 6(d). The Al and Ga gradients in the EDX maps show that the Al atoms diffused from the sapphire substrate to the $(AlGa)_2O_3$ layer, which is the opposite of the Ga diffusion. Meanwhile, the O distribution was homogeneous. In Figs. 6(b) and 6(d), the EDX signal overlap maps show a tiny orange region comprising Al red and Ga green signals at the interface of β-$(AlGa)_2O_3$/sapphire, reaffirming the existence of the transition layer. For the EDX spectra in Figs. 6(b) and 6(d), the signal intensity of Al is weaker than that of Ga for the sample annealed at 1000 °C in Fig. 6(b) amid the β-$(AlGa)_2O_3$ layer. However, it is stronger than that of Ga for the sample annealed at 1400 °C in Fig. 6(d). The results reiterate that with higher annealing temperatures, more Al atoms could diffuse into the $AlGa_2O_3$ layer, leading to higher Al contents. It is noted that because the film thickness increased amid the annealing due to the interdiffusion process, one could design experiments with different initial thicknesses and contents to reach the desired thicknesses and contents by utilizing the knobs of the annealing temperature and perhaps the annealing time.

In summary, based on the binary β-Ga_2O_3/sapphire templates, we have employed the thermal annealing method at 1000–1500 °C to demonstrate ternary β-$(Al_xGa_{1-x})_2O_3$ films with wide ranges of optical bandgaps and compositions. Higher annealing temperatures resulted in larger Al contents for the β-$(Al_xGa_{1-x})_2O_3$ films. The optical bandgap range of the samples was 4.88–6.38 eV translating to the Al content range of 0–0.72 for the β-Ga_2O_3 templates without annealing and with annealing up to 1400 °C. Evaluated by XRD, the Al content range of the samples was 0–0.81 for the templates without annealing and with annealing up to 1500 °C. The ternary alloy formation was caused by the interdiffusion of Ga and Al atoms from the thin film and substrate, respectively, which was proportional to the annealing temperatures. The interdiffusion was confirmed by SIMS and TEM. The Al contents of β-$(Al_xGa_{1-x})_2O_3$ ternary thin films were highly homogeneous with higher temperatures ($\geq$1200 °C). The Ga atoms diffused concurrently into the sapphire substrate during the annealing, resulting in an increased β-$(AlGa)_2O_3$ film thickness compared to the β-Ga_2O_3 templates. Besides, the crystal quality of β-$(Al_xGa_{1-x})_2O_3$ could improve significantly amid higher temperature annealing. Since the annealing temperature is an excellent knob to control the bandgap and composition, one could design a proper initial thickness and composition of binary β-Ga_2O_3 and β-$(AlGa)_2O_3$ to reach the desired thickness and composition of ternary β-$(AlGa)_2O_3$ films by utilizing the annealing technique. The proposed method does not involve the direct-growth techniques for alloys and, therefore, is promising for straightforward and low-cost production of the high-quality β-$(AlGa)_2O_3$ alloys.

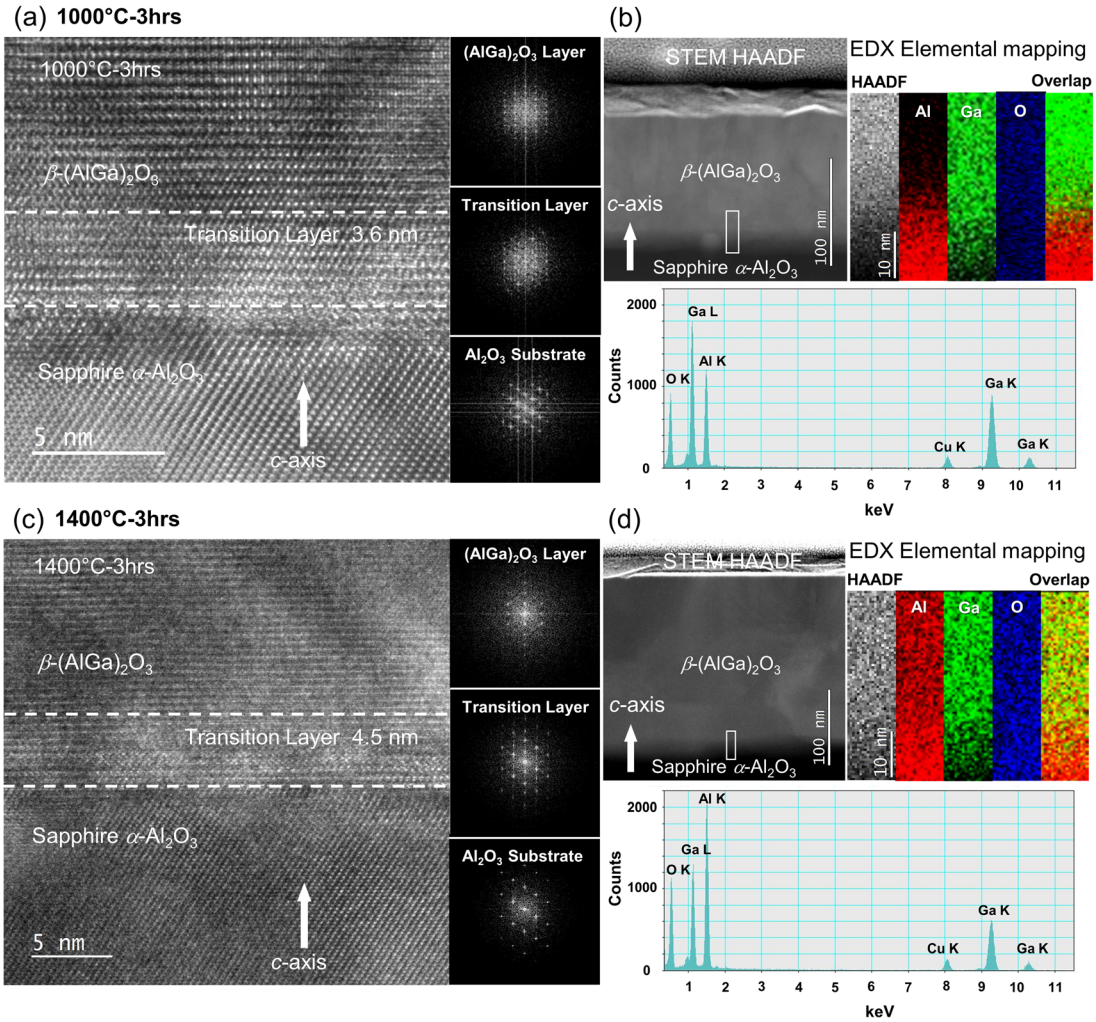

FIG. 6. Cross-sectional HR-TEM images and the FFT diffraction patterns in the vicinity of the β-$(AlGa)_2O_3$/sapphire interface of the samples annealed at (a) 1000 °C and (c) 1400 °C. The corresponding HAADF images, EDX maps, and EDX spectra in the vicinity of the transition region (white rectangular area) are shown in (b) and (d).

See the supplementary material for XRD phi-scan of the (−401) plane and a table summary of XRD (−201) rocking curve FWHMs and $5 \times 5\ \mu m^2$ AFM RMS surface roughness of the samples.

The authors would like to acknowledge the support of KAUST Baseline BAS/1/1664-01-01, GCC Research Council REP/1/3189-01-01, and Competitive Research Grant Nos. URF/1/3437-01-01 and URF/1/3771-01-01.

DATA AVAILABILITY

The data that support the findings of this study are available within this article and its supplementary material.

REFERENCES

[1]M. Higashiwaki and G. H. Jessen, Appl. Phys. Lett. **112**, 060401 (2018).
[2]T. Oshima, T. Okuno, N. Arai, N. Suzuki, H. Hino, and S. Fujita, Jpn. J. Appl. Phys., Part 1 **48**, 011605 (2009).
[3]T. Oshima, T. Okuno, and S. Fujita, Jpn. J. Appl. Phys., Part 1 **46**, 7217 (2007).
[4]D. Guo, Z. Wu, P. Li, Y. An, H. Liu, X. Guo, H. Yan, G. Wang, C. Sun, L. Li, and W. Tang, Opt. Mater. Express **4**, 1067 (2014).
[5]F. Yu, S. Ou, and D. Wuu, Opt. Mater. Express **5**, 1240 (2015).
[6]Z. Feng, L. Huang, Q. Feng, X. Li, H. Zhang, W. Tang, J. Zhang, and Y. Hao, Opt. Mater. Express **8**, 2229 (2018).
[7]A. S. Pratiyush, S. Krishnamoorthy, S. Kumar, Z. Xia, R. Muralidharan, S. Rajan, and D. N. Nath, Jpn. J. Appl. Phys., Part 1 **57**, 060313 (2018).
[8]D. Guo, H. Liu, P. Li, Z. Wu, S. Wang, C. Cui, C. Li, and W. Tang, ACS Appl. Mater. Interfaces **9**, 1619 (2017).
[9]M. Higashiwaki, H. Murakami, Y. Kumagai, and A. Kuramata, Jpn. J. Appl. Phys., Part 1 **55**, 1202A1 (2016).
[10]C. G. Torres-Castanedo, K. H. Li, L. Braic, and X. Li, J. Phys. D: Appl. Phys. **53**, 314003 (2020).
[11]H. Sun, C. G. T. Castanedo, K. Liu, K.-H. Li, W. Guo, R. Lin, X. Liu, J. Li, and X. Li, Appl. Phys. Lett. **111**, 162105 (2017).
[12]M. Higashiwaki, K. Sasaki, A. Kuramata, T. Masui, and S. Yamakoshi, Appl. Phys. Lett. **100**, 013504 (2012).
[13]K. Konishi, K. Goto, H. Murakami, Y. Kumagai, A. Kuramata, S. Yamakoshi, and M. Higashiwaki, Appl. Phys. Lett. **110**, 103506 (2017).

[14]S. Krishnamoorthy, Z. Xia, S. Bajaj, M. Brenner, and S. Rajan, Appl. Phys. Express **10**, 051102 (2017).
[15]A. J. Green, K. D. Chabak, M. Baldini, N. Moser, R. Gilbert, R. C. Fitch, G. Wagner, Z. Galazka, J. Mccandless, and A. Crespo, IEEE Electron Device Lett. **38**, 790 (2017).
[16]R. Roy, V. G. Hill, and E. F. Osborn, J. Am. Chem. Soc. **74**, 719 (1952).
[17]H. Aida, K. Nishiguchi, H. Takeda, N. Aota, K. Sunakawa, and Y. Yaguchi, Jpn. J. Appl. Phys., Part 1 **47**, 8506 (2008).
[18]N. Suzuki, S. Ohira, M. Tanaka, T. Sugawara, K. Nakajima, and T. Shishido, Phys. Status Solidi C **4**, 2310 (2007).
[19]Z. Galazka, R. Uecker, K. Irmscher, M. Albrecht, D. Klimm, M. Pietsch, M. Brützam, R. Bertram, S. Ganschow, and R. Fornari, Cryst. Res. Technol. **45**, 1229 (2010).
[20]Y. Kokubun, K. Miura, F. Endo, and S. Nakagomi, Appl. Phys. Lett. **90**, 031912 (2007).
[21]M. Ogita, N. Saika, Y. Nakanishi, and Y. Hatanaka, Appl. Surf. Sci. **142**, 188 (1999).
[22]D. H. Kim, S. H. Yoo, T.-M. Chung, K.-S. An, H.-S. Yoo, and Y. Kim, Bull. Korean Chem. Soc. **23**, 225 (2002).
[23]Y. Xu, Z. An, L. Zhang, Q. Feng, J. Zhang, C. Zhang, and Y. Hao, Opt. Mater. Express **8**, 2941 (2018).
[24]M. Orita, H. Hiramatsu, H. Ohta, M. Hirano, and H. Hoson, Thin Solid Films **411**, 134 (2002).
[25]E. G. Víllora, K. Shimamura, K. Kitamura, and K. Aoki, Appl. Phys. Lett. **88**, 031105 (2006).
[26]H. Sun, K. Li, C. G. T. Castanedo, S. Okur, G. S. Tompa, T. Salagaj, S. Lopatin, A. Genovese, and X. Li, Cryst. Growth Des. **18**, 2370 (2018).
[27]T. Wang, W. Li, C. Ni, and A. Janotti, Phys. Rev. Appl. **10**, 011003 (2018).
[28]H. Lee, J. Liu, and C. Lee, IEEE Photonics Technol. Lett. **30**, 549 (2018).
[29]X. Wang, Z. Chen, F. Zhang, K. Saito, T. Tanaka, M. Nishio, and Q. Guo, AIP Adv. **6**, 015111 (2016).
[30]F. Zhang, K. Saito, T. Tanaka, M. Nishio, M. Arita, and Q. Guo, Appl. Phys. Lett. **105**, 162107 (2014).
[31]J. Shi, H. Liang, X. Xia, Z. Long, H. Zhang, Y. Liu, X. Dong, and Z. Jia, ECS J. Solid State Sci. Technol. **9**, 045016 (2020).
[32]H. Ito, K. Kaneko, and S. Fujita, Jpn. J. Appl. Phys., Part II **51**, 09LD16 (2012).
[33]D. Tahara, H. Nishinaka, S. Morimoto, and M. Yoshimoto, Appl. Phys. Lett. **112**, 152102 (2018).
[34]J. Li, X. Chen, T. Ma, X. Cui, F.-F. Ren, S. Gu, R. Zhang, Y. Zheng, S. P. Ringer, L. Fu, H. H. Tan, C. Jagadish, and J. Ye, Appl. Phys. Lett. **113**, 041901 (2018).
[35]Q. Feng, X. Li, G. Han, L. Huang, F. Li, W. Tang, J. Zhang, and Y. Hao, Opt. Mater. Express **7**, 1240 (2017).
[36]R. Miller, F. Alema, and A. Osinsky, IEEE Trans. Semicond. Manuf. **31**, 467 (2018).
[37]A. F. M. A. U. Bhuiyan, Z. Feng, J. M. Johnson, H.-L. Huang, J. Sarker, M. Zhu, M. R. Karim, B. Mazumder, J. Hwang, and H. Zhao, APL Mater. **8**, 031104 (2020).
[38]A. F. M. A. U. Bhuiyan, Z. Feng, J. M. Johnson, H.-L. Huang, J. Hwang, and H. Zhao, Cryst. Growth Des. **20**, 6722 (2020).
[39]A. F. M. A. U. Bhuiyan, Z. Feng, J. M. Johnson, H.-L. Huang, J. Hwang, and H. Zhao, Appl. Phys. Lett. **117**, 142107 (2020).
[40]T. Oshima, T. Okuno, N. Arai, Y. Kobayashi, and S. Fujita, Jpn. J. Appl. Phys., Part 1 **48**, 070202 (2009).
[41]M. Fleischer, W. Hanrieder, and H. Meixner, Thin Solid Films **190**, 93 (1990).
[42]G. A. Battiston, R. Gerbasi, M. Porchia, R. Bertoncello, and F. Caccavale, Thin Solid Films **279**, 115 (1996).
[43]A. Goyal, B. S. Yadav, O. P. Thakur, A. K. Kapoor, and R. Muralidharan, J. Alloys Compd. **583**, 214 (2014).
[44]H. Li, S.-H. Yuan, T.-M. Huang, H.-J. Chen, F.-H. Lu, S. Zhang, and D.-S. Wuu, J. Alloys Compd. **823**, 153755 (2020).
[45]C. Kranert, M. Jenderka, J. Lenzner, M. Lorenz, H. von Wenckstern, R. Schmidt-Grund, and M. Grundmann, J. Appl. Phys. **117**, 125703 (2015).
[46]H. Peelaers, J. B. Varley, J. S. Speck, and C. G. Van de Walle, Appl. Phys. Lett. **112**, 242101 (2018).
[47]H. Peelaers, J. B. Varley, J. S. Speck, and C. G. Van de Walle, Appl. Phys. Lett. **115**, 159901 (2019).